Divertor Heat Flux Mitigation in High-Performance H-mode Plasmas in the National Spherical Torus Experiment.

V. A. Soukhanovskii 1), R. Maingi 2), D. A. Gates 3), J. E. Menard 3), S. F. Paul 3), R. Raman 4), A. L. Roquemore 3), R. E. Bell 3), C. E. Bush 2), R. Kaita 3), H. W. Kugel 3), B. P. LeBlanc 3), D. Mueller 3), and the NSTX Research Team.
1) Lawrence Livermore National Laboratory, Livermore, CA, USA
2) Oak Ridge National Laboratory, Oak Ridge, TN, USA
3) Princeton Plasma Physics Laboratory, Princeton, NJ, USA
4) University of Washington, Seattle, WA, USA
Email address of main author: vlad@llnl.gov

Abstract. Experiments conducted in high-performance 1.0-1.2 MA 6 MW NBI-heated H-mode plasmas with a high flux expansion radiative divertor in NSTX demonstrate that significant divertor peak heat flux reduction and access to detachment may be facilitated naturally in a highly-shaped spherical torus (ST) configuration. Improved plasma performance with high $\beta_p = 15 - 25$ %, a high bootstrap current fraction $f_{BS} = 45 - 50$ %, longer plasma pulses, and an H-mode regime with smaller ELMs has been achieved in the lower single null configuration with higher-end elongation 2.2-2.4 and triangularity 0.6-0.8. Divertor peak heat fluxes were reduced from 6-12 MW/m^2 to 0.5-2 MW/m^2 in ELMy H-mode discharges using high magnetic flux expansion and partial detachment of the outer strike point at several D_2 injection rates, while good core confinement and pedestal characteristics were maintained. The partially detached divertor regime was characterized by a 30-60 % increase in divertor plasma radiation, a peak heat flux reduction by up to 70 %, measured in a 10 cm radial zone, a five-fold increase in divertor neutral pressure, and a significant volume recombination rate increase.

1. Introduction

Candidate techniques for steady-state mitigation of divertor heat and particle fluxes in future fusion plasma devices must be capable of reducing particle fluxes to the levels of acceptable divertor plate material erosion rates and heat fluxes to $q \simeq 10$ MW/m^2, a limit imposed by the present day divertor material and engineering constrains. The techniques must also be compatible with high-performance high-confinement core plasmas and particle control methods. Presently both passive (divertor geometry) and active (radiative divertors, field ergodization) techniques are considered as candidate mitigation strategies for ITER and next step fusion devices [1] - [5]. Radiative divertors use deuterium and impurities to reduce particle and heat fluxes by means of volumetric momentum and energy dissipative processes - the ion-neutral elastic and inelastic collisions, recombination and radiative cooling [1]. Specialized divertor configurations rely on the poloidal magnetic flux expansion to reduce particle and heat flux density on divertor targets, as well as the target inclination in respect to the incident field lines, and the extended connection length to radiate additional power. Closely coupled to the development of the mitigation techniques are experimental studies of the scrape-off layer (SOL) transport and turbulence that provide validation of divertor models and novel designs [1, 6].

Substantial experimental work has been carried out on the radiative divertor and divertor geometry effects in tokamaks [1, 6]. In a low aspect ratio spherical torus (ST) magnetic geometry, an inherently large divertor figure of merit P/R [7] (where P is input power and R is major radius) and a number of ST SOL/divertor geometry features

lead to high divertor heat fluxes [8, 9], raising concerns over divertor operation in the proposed ST-based concepts, e.g., the Component Test Facility (CTF) [3] and National High-power Advanced Torus eXperiment (NHTX) [4]. Both of the concepts employ the radiative divertor and/or mantle with high radiated power fractions. This paper reports on the recent radiative divertor experiments in the National Spherical Torus Experiment (NSTX). Significant peak heat flux reduction simultaneously with good core plasma confinement have been demonstrated in high performance 1.0-1.2 MA 6 MW NBI-heated H-mode discharges. Access to the radiative divertor regime was previously studied in NSTX in 2-6 MW NBI-heated H-mode discharges in a weakly shaped lower single null (LSN) configuration (a range of elongations $\kappa = 1.8 - 2.0$ and triangularities $\delta = 0.40 - 0.50$) using a high D_2 injection rate generally incompatible with H-mode confinement [10, 11]. Experiments conducted in $0.8 - 1.0$ MA $4 - 6$ MW NBI-heated H-mode discharges in a highly-shaped LSN configuration, however, demonstrated reliable access to the partially detached divertor (PDD) regime. The peak heat flux q_{pk} at the outer strike point (SP) was successfully reduced from 4-6 MW/m^2 to 0.5-2 MW/m^2 using divertor deuterium injection with minimal confinement deterioration [12].

2. Experiment

A comprehensive SOL and divertor diagnostic set has been developed on NSTX (Fig. 1) as described in detail in Refs. [10] -[12]. Recent facility and diagnostic upgrades were aimed at 1) improved control of divertor gas injection and 2) improved measurements of radiation and neutrals to elucidate on the power and momentum balance in the divertor. These upgrades are briefly described as follows. A new divertor gas injector with a piezoelectric valve enabled injection of D_2 into the outer SOL at a constant flow rate up to 200 Torr l / s (1.4×10^{22} s^{-1}). The flow rate was controlled by prefilling the injector plenum to a certain calibrated pressure. To add the spatial resolution to impurity and deuterium line emission measurements, a new 10-fiber interface was developed for the divertor UV-VIS spectrometer [13]. An upgrade to the divertor bolometer system included new detectors and also provided higher spatial resolution of the radiated power measurements in the outer divertor leg. An additional Penning gauge was installed in the outer divertor region, to complement the existing midplane and divertor pressure measurements [14]. The neutral pressure measurements were not conductance-limited.

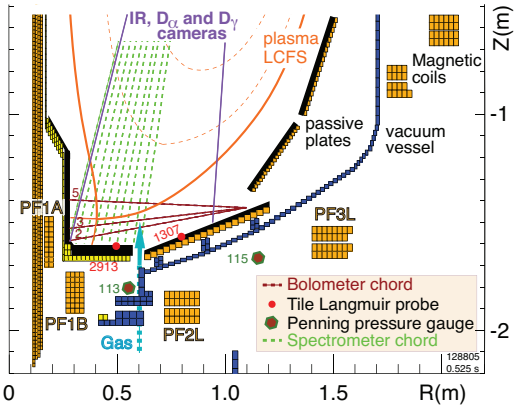

Figure 1: *Layout of divertor diagnostics.*

The NSTX plasma control system [15, 16] was used to obtain a highly-shaped LSN configuration with $\kappa \simeq 2.2 - 2.3$, $\delta \simeq 0.8$, and the δ_{rsep} parameter, the midplane distance between the primary and the secondary separatrices, between 8 and 12 mm. The ion ∇B drift direction was toward the lower X-point. In this configuration, the inner SP was located on the vertical graphite tile target (inner wall), while the outer SP was located on the horizontal graphite target. A salient feature of this configuration was a high (18-26) magnetic flux expansion evaluated at the outer SP. Experiments were conducted at $B_t = 0.45$ T. The core plasma conditions were: $T_e(0) \simeq (0.8 - 1.2)$ keV, $\bar{n}_e \simeq (5 - 7) \times 10^{19}$ m^{-3}.

3. High-performance H-mode discharges with radiative divertor

Improved plasma performance approaching the performance level of CTF with high $\beta_t = 15 - 25$ %, high $\beta_N \leq 5.7$, and a high bootstrap current fraction $f_{BS} = 45 - 50$ % sustained for several current redistribution times has been achieved in highly-shaped plasmas in NSTX [15, 17]. Radiative divertor experiments conducted in this configuration also demonstrated the benefits of increased shaping for divertor heat flux management. The high divertor magnetic flux expansion led to reduced particle and heat fluxes on the divertor plate, and provided a facilitated access to outer SP detachment [12]. In this work we demonstrate successful radiative divertor operation in high-performance 1.0-1.2 MA H-mode discharges with 6 MW NBI heating. Steady-state measurements of divertor heat flux in the NSTX at low κ, δ showed that q_{pk} increased monotonically with P_{NBI} and I_p, whereas the heat flux width λ_q decreased with I_p [18]. To the first order, the q_{pk} dependence is understood as the corresponding increase in P_{SOL} from the external and ohmic heating powers, and the decrease in connection length $L_\parallel$ ($L_\parallel$ is proportional to the safety factor q). Because $q_\parallel = P_{SOL}/A_\perp = P_{SOL}/(4\pi R(B_p/B_{tot})\lambda_q)$, the discharges with $I_p = 1.0 - 1.2$ MA and $P_{NBI} = 6$ MW represent a challenging case with the highest $q_\parallel$, estimated to be 50-80 MW/m^2. The radiative divertor technique employed divertor D_2 injection that increased divertor density, recycling and neutral pressure. The associated increases in radiated power and ion momentum loss through charge exchange, elastic collisions, and eventually recombination, led to a reduction in heat and particle fluxes in the outer SP region. Presented below are SOL and divertor measurements that contributed to a consistent picture of the PDD regime in NSTX.

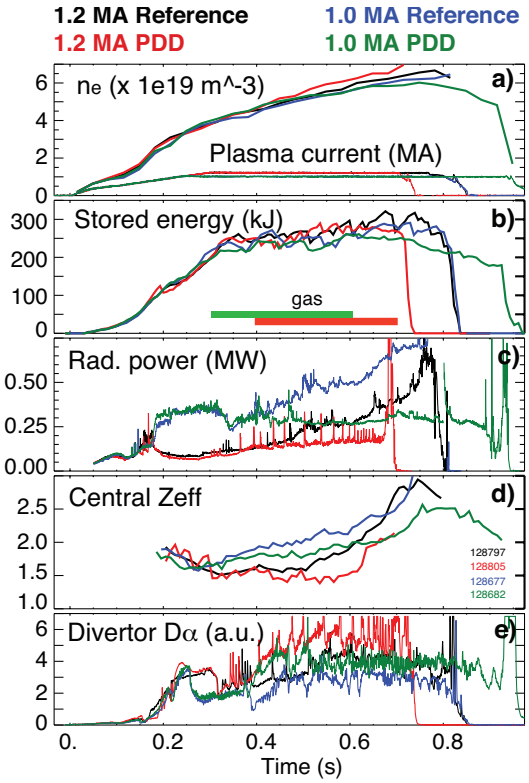

Figure 2: *Time traces of 1.0 MA and 1.2 MA 6 MW discharges with and without divertor gas injection.*

Demonstration of the radiative divertor operation on NSTX with minimal core and pedestal plasma performance degradation was an important objective of the experiment. Core conditions are illustrated for the reference 1.0 MA and 1.2 MA 6 MW H-mode discharges and for the discharges with divertor D_2 injection in Fig. 2. A transition to the PDD regime occurred within 30-50 ms from the start of the D_2 injection. Thomson scattering profiles showed that pedestal T_e decreased and n_e increased by 5-15 %. Core plasma stored energy degraded by 5-15 % during the PDD phase. The energy confinement time in the H-mode phase was $\tau_E \simeq 40 - 60$ ms, being in the range 1.6-1.8 of the the ITER89P confinement scaling factor. As in previous radiative divertor experiments in NSTX [10, 12], the change in divertor conditions had a pronounced effect on core carbon concentration and radiated power. Plasma Z_{eff} was in the range 1.5-2.5. The main impurity identified by VUV and UV spectroscopy was carbon. Both P_{rad} and Z_{eff} decreased substantially, by 20-30 %, during the PDD phase.

Part of this decrease could be attributed to the large Type I ELMs that appeared as a result of the gas puffing in the 1.2 MA discharges. However, in the 1.0 MA discharges, gas puffing did not affect the reference, small ELM regime, suggesting that the carbon divertor source was also reduced during the detachment.

Partial detachment of the outer SP was obtained at several gas puffing rates Γ_g. Summarized in Fig. 3 are the peak heat flux q_{pk} measurements at progressive times for a number of gas puffing rates. For comparison, measurements of highest q_{pk} in reference discharges (without gas injection) are also shown. In general, higher gas puffing rates were necessary to reduce q_{pk} in 1.2 MA discharges, where $q_{\|}$ was higher, in comparison with 1.0 MA discharges, as expected from the dependence of $q_{\|}$ and λ_q on I_p. As evident from the figure, higher Γ_g led to a faster q_{pk} reduction, however, after about 250-270 ms peak heat fluxes reached steady-state low levels, being about 1 MW/m^2 in the 1.0 MA discharges, and about 1.5-2.0 MW/m^2 in the 1.2 MA discharges.

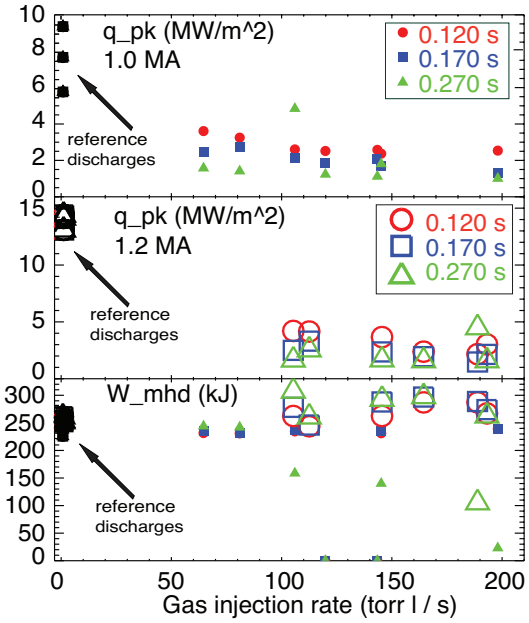

Figure 3: *Divertor q_{pk} in (a) 1.0 MA and (b) 1.2 MA PDD discharges as a function of gas injection rate at 120 ms, 170 ms, and 270 ms after the start of gas injection. Panel (c) shows plasma stored energy for the same discharges and times.*

Optimization through gas injection entailed using the rate and gas pulse duration that reduced q_{pk} on a time scale of 100-200 ms yet caused minimal reduction in confinement and did not lead to an X-point MARFE formation over 0.5-0.7 s. For the 1.0 MA discharges, this rate was found to be $\Gamma_g \leq 100$ Torr l /s, while for 1.2 MA discharges it was in the range 110-160 Torr l /s, as follows from the stored energy trend in Fig. 3 (c). This experience was similar to early tokamak experiments with open geometry divertors operated without active pumping [1].

Divertor gas injection increased local divertor density and divertor radiation, and as a result, q_{pk} was substantially decreased. Shown in Fig. 4 are divertor heat flux profiles for the 1.0 MA and 1.2 MA discharges discussed above. In both cases, a 40-70 % decrease in heat flux was measured in a $9-11$ cm radial zone adjacent to the outer SP. The extent of the detachment zone was within 70-80 % of the full divertor SOL width. Heat flux profiles did not change outside of the detachment zone, remaining at a level 0.5-1.0 MW/m^2.

Divertor characteristics pertaining to the divertor power and momentum balances will be now discussed using the 1.2 MA PDD discharge data. Time traces of the SOL and divertor power balance elements for the 1.2 MA case are shown in Fig. 5. They confirmed that plasma radiation accounted for much of the divertor power loss. From the total SOL power of $P_{SOL} = 4.5-5$ MW, the outer divertor received about 2-3 MW in the reference discharge, and 1-2 MW in the PDD discharge. The power flow into the detached inner divertor and the upper divertor were both negligible, confirmed by IR camera measurements. While it was not possible to fully account for the lower divertor radiation with the present bolometer coverage, divertor bolometer signals representative of the outer divertor leg did show substantial radiated power increase (Fig. 5 (c)). An estimate of the outer leg radiated power using an average plasma irradiance of 25 W/cm^2 and the outer leg volume 0.1 m^3

yielded about 0.5 MW of radiated power, being within 10 % of the total P_{SOL}. Intrinsic carbon impurity and deuterium were identified as the main radiating species responsible for divertor power loss. Shown in Fig. 5 (d) is the brightness contour of the C II $\lambda = 375$ nm line representative of the C II emission distribution in the divertor. Also shown is the outer SP location and a projection of the X-point on the divertor surface. A significant increase in C II emission was correlated with the PDD regime onset. The emission was concentrated in the SP region throughout the outer divertor leg, and increased continuously during the gas injection phase. Toward the end of the discharge, the emission peaked around the X-point, suggesting that an X-point MARFE may have formed.

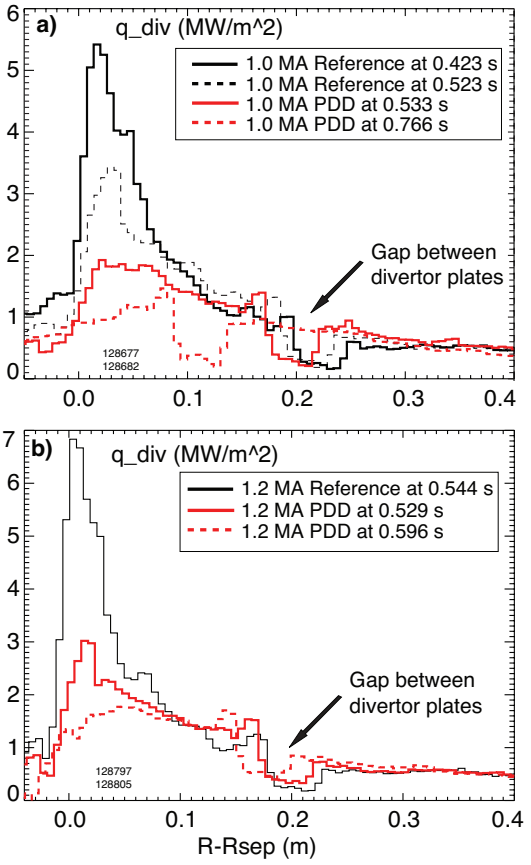

Figure 4: *Divertor heat flux profiles in the reference and PDD discharges - (a) 1.0 MA, (b) 1.2 MA*

During the detachment, particle flux to the plate is reduced due to the plasma parallel pressure loss. Experimentally, this is evidenced by the Langmuir probe ion saturation current "roll-over", or in some cases, constant value, in the detachment zone, while the divertor D_α intensity continues to increase [1]. Shown in Fig. 6 (a), (b) are the I_{sat} time traces of two divertor Langmuir probes. Probe locations are shown in Fig. 1. Probe 2913 was located at 9-11 cm from the OSP, marginally inside the PDD zone. Its I_{sat} remained low during the gas injection and OSP detachment, and eventually reduced, while D_α intensity increased. Probe 1307 was located outside of the divertor SOL.The increase of its I_{sat}, as well as the D_α intensity, were well correlated with the gas injection, suggesting that the far SOL was in the high-recycling regime.

Plasma pressure loss during detachment is caused by ion momentum loss due to ion-neutral elastic collisions, charge exchange and electron-ion volumetric recombination. For the former two to occur at a substantial rate, a high neutral density must be maintained in the divertor. Time traces of neutral pressure measurements by the Penning gauges located in the outer divertor region are shown in Fig. 6 (c) and (d). A high neutral pressure, $p_n = 0.5 - 1.5$ mTorr, was maintained in the divertor during the PDD phase.

Partial detachment zone is characterized by a formation of a very low T_e and high n_e region adjacent to the divertor plate. The radiative and the three-body recombination can also act as a momentum sink for plasma ions. The recombination rate is a strong function of temperature and density, being low $R \leq 5 \times 10^{-19}$ m^3 s^{-1} at $T_e \geq 1.5$ eV and $n_e \leq 5 \times 10^{19}$ m^{-3}, however, much higher when T_e decreases and n_e increases beyond these values. The experimental signature of recombination is the appearance and/or intensity increase of the D I $n = 6 - 11$ Balmer lines. Based on the developed Stark broadening and line intensity analysis [12, 13], the average plasma conditions in the PDD zone were estimated to be $n_e \leq 3 - 5 \times 10^{20}$ m^{-3}, and low $T_e \leq 1.5$ eV. Shown in Fig. 6 (e) is the Balmer D10 line brightness contour as a function of time and divertor radius. A region of volume recombi-

nation formed following the gas injection, and increased in the spatial extent and rate concomitantly with the neutral pressure rise. The Langmuir probe 2913 location is also shown. The expansion of the recombination region was well correlated with the the probe I_{sat} "roll-over", suggesting further studies of the role of recombination in the ion balance during the PDD phase. The Balmer D10 line emission appeared to peak in the X-point region, consistent with the notion of a possible MARFE formation.

4. Discussion

We have demonstrated experimentally that significant peak heat flux reduction simultaneously with high core plasma performance and confinement could be achieved in a high input power high current ST using the radiative divertor technique. The radiative divertor was induced by a moderate-rate D_2 injection and radiation from intrinsic carbon. The significance of this result is that it was obtained in a highly-shaped horizontal plate divertor configuration without active pumping, suggesting that in high performance highly-shaped ST plasmas access to reduced divertor heat flux is naturally facilitated by SOL and divertor geometry effects. The openness of the divertor configuration is an additional benefit enabling much flexibility in plasma shaping optimization.

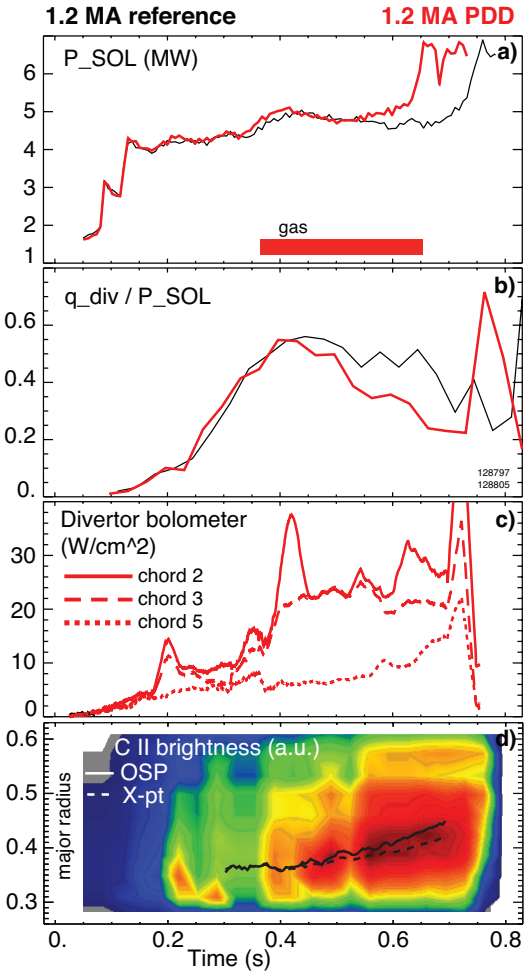

Figure 5: *Time traces of a reference and a PDD 1.2 MA discharges (a) P_{SOL}, (b) Q_{div}/P_{SOL}, (c) Divertor bolometer signals, (e) C II brightness distribution in divertor.*

Scrape-off layer and divertor geometry effects appear to play a prominent role in divertor transport in NSTX. Shown in Table 1 are divertor parameters of the highly-shaped NSTX configuration and for comparison, typical divertor parameters of a large aspect ratio tokamak, such as, e.g. DIII-D. Evident are several ST geometry features that explain the observed divertor heat flux trends in NSTX. First, a large in-out plasma surface area asymmetry in NSTX, along with a large Shafranov shift resulting in steep outboard gradients, lead to the heat flow distribution mostly into the outer SOL region. Second, a higher angle between B field lines and the divertor surface means that for the same $q_{||}$ the deposited heat flux would be generally higher in an ST than in the tokamak. Third, a relatively short parallel connection length L_x between the X-point and divertor target leads to reduced radiated power and momentum losses. The fraction of $q_{||}$ that can be radiated is a strong function of L_x for the given impurity radiation function L_Z [19]. The momentum loss is also a function of L_x. In a shorter parallel connection length divertor, fewer ions would be able to undergo a collision with a neutral and a recombination event before striking the divertor surface. Finally, because of a large magnetic shear in the ST, there is a large radial gradient of the parallel connection length $\partial L_x/\partial r$. The connection length, being relatively short in the separatrix region

$L_x = 5 - 8$ m, becomes very short, $L_x \sim 1$ m, at a radial distance of one SOL width λ_q. A steep decline in L_x suggests that significant power and momentum losses can be sustained only in the radial region adjacent to the separatrix, while power and particle fluxes in the far SOL may be impossible to reduce.

The experimental results were interpreted using the two point SOL heat transport model with losses [10], a one-dimensional heat conduction SOL model with non-coronal impurity radiation [12, 19], and the five region SOL model with constant power and particle sources and sinks [12, 20]. The models semi-quantitatively explained all observed features of the divertor regimes in NSTX. The models predicted that large radiated power fractions and parallel momentum loss fractions were needed to reach the detachment in NSTX. The models did not include the 2D divertor geometry effects, thought to be essential for the apparently easy access to the outer SP detachment in highly-shaped plasmas. The high flux expansion divertor in NSTX has a high physical divertor volume and apparently, a higher plasma "plugging efficiency". The plasma "plugging efficiency" ζ is defined as a fraction of recycling neutrals re-ionized in the divertor region. In the high flux expansion divertor ζ is higher because of the larger divertor plasma size in physical space, higher low-temperature plasma volume, and thus reduced transparency to neutrals.

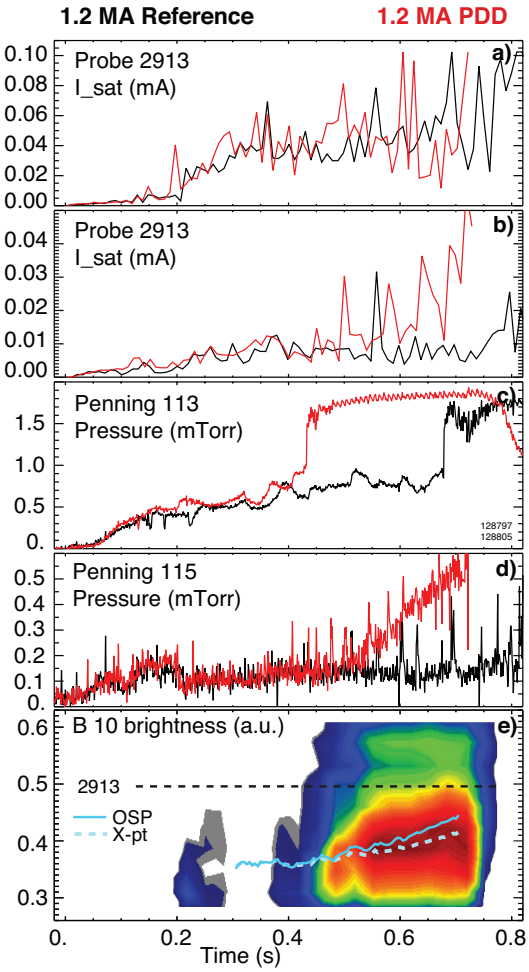

Figure 6: *Time traces of (a) I_{sat} of Langmuir probe 2913, (b) I_{sat} of Langmuir probe 1307, (c) neutral pressure in outer divertor region, (d) neutral pressure in outer divertor region, (d) brightness of the D I 10-4 line a 1.2 MA reference and a PDD discharges.*

The geometric features of the ST SOL and divertor discussed above help explain the observed general divertor characteristics in NSTX. While highly radiative, reduced divertor heat flux discharges are not uncommon in NSTX, the PDD regime appeared to be accessible only with additional gas injection and only in the highly-shaped configuration [10, 12]. It also appears that $\bar{n}_e$ is weakly coupled with n_{sep} in NSTX as compared to conventional large aspect ratio tokamaks. In NSTX, the $\bar{n}_e$ increases are quite common, however, n_{sep} does not increase proportionally even when $\bar{n}_e$ approaches the Greenwald value. This explains in part why the PDD regime does not occur spontaneously as a result of the ramping density, as the SOL collisionality remains at a fairly low value $\nu^*_{SOL,e} \sim 10 - 30$ (estimated).

Many similarities in the PDD regime properties between NSTX and conventional large aspect ratio tokamaks [21] were found. The PDD regime was characterized by a peak heat flux reduction due to radiating intrinsic carbon impurity. Also evident was

Quantity	NSTX	Tokamak
Aspect ratio	1.4-1.5	2.7
In-out plasma boundary area ratio	1:3	2:3
Midplane to target connection length L_c (m)	8-10	30-80
X-point to target parallel length L_x (m)	5-7	10-20
X-point to target poloidal length L_p (m)	0.05-0.15	0.05-0.25
Poloidal magnetic flux expansion f_m at OSP	16-24	3-15
Magnetic field angle at target (degree)	2-5	1-2

Table 1: Typical SOL and divertor geometric factors of the high κ, δ configuration of NSTX and a tokamak.

a particle flux reduction, apparently due to the pressure loss along the flux tube caused by ion momentum loss, and a formation of an expanding region of high-rate volume recombination. Also consistent with tokamak experiments, continuous gas injection eventually resulted in an increase of the divertor density beyond a critical n_e value of the X-point MARFE, which in turn degraded the confinement and terminated the discharge. A further optimization of the radiative divertor regime in NSTX would apparently be possible only with active pumping of the divertor density.

Summary

Successful divertor peak heat flux mitigation in a high power density ST with a simultaneous high core plasma confinement properties has been demonstrated in NSTX using the radiative divertor technique. Divertor peak heat flux scaling developed for NSTX show monotonic dependence on input power (and P_{SOL}) and plasma current I_p. In the highest achievable range of $P_{NBI} = 6$ MW and $I_p = 1.0 - 1.2$ MA, divertor peak heat flux was reduced from 6-12 MW/m^2 to 0.5-2 MW/m^2 using high magnetic flux expansion and partial detachment of the outer strike point. This, in combination with an attractive small ELM [22] high-β, high bootstrap current fraction regime [17] H-mode plasma scenario will form a basis for high-performance scenario development for the future ST-based concepts, such as the CTF [3] and NHTX [4].

Acknowledgements We thank the entire NSTX Team for technical, engineering and computer support as well as for plasma, NBI and diagnostic operations. This work was performed under the auspices of the U.S. Department of Energy under Contracts DE-AC52-07NA27344, DE-AC02-76CH03073, DE-AC05-00OR22725, W-7405-ENG-36, and DE-FG02-04ER54758.

References

[1] ITER PHYSICS EXPERT GROUP ON DIVERTOR et al., Nuc. Fusion **39** (1999) 2391.
[2] ASAKURA, N. et al., in *Proc. 34th EPS Conference on Plasma Physics*, edited by GASIOR, P., volume 31F of *Europhys. Conf. Abstr.*, pages P–1.051, Warsaw, Poland, 2007.
[3] PENG, Y.-K. et al., Plasma Phys. Control. Fusion **47** (2005) 263.
[4] GOLDSTON, R. J. et al., Paper FT/P3-12 (This conference).
[5] RYUTOV, D. D. et al., Paper IC/P4-8 (This conference).
[6] LOARTE, A. et al., Nucl. Fusion **47** (2007) S203.
[7] LACKNER, K., Comments Plasma Physics Control. Fusion **15** (1994) 359.
[8] MAINGI, R. et al., Nucl. Fusion. **43** (2003) 969.
[9] MAINGI, R. et al., J. Nucl. Mater. **313-316** (2003) 1005.
[10] SOUKHANOVSKII, V. A. et al., in *Proc. 21st FEC*, Paper EX/P4–28, Chengdu, China, 2006, IAEA.
[11] SOUKHANOVSKII, V. A. et al., J. Nucl. Mater. **363-365** (2007) 432.
[12] SOUKHANOVSKII, V. A. et al., Paper BI1.00005, Bull. Am. Phys. Soc. **52** (2007) Submitted to Phys. Plasmas.
[13] SOUKHANOVSKII, V. A. et al., Rev. Sci. Instrum. **77** (2006) 10F127.
[14] RAMAN, R. et al., Rev. Sci. Instrum. **75** (2004) 4347.
[15] GATES, D. et al., Phys. Plasmas **13** (2006) 056122.
[16] GATES, D. et al., Nucl. Fusion **46** (2006) 22.
[17] MENARD, J. et al., Nucl. Fusion **47** (2007) 645.
[18] MAINGI, R. et al., J. Nucl. Mater. **363-365** (2007) 196.
[19] POST, D. et al., J. Nucl. Mater. **220-222** (1995) 1014.
[20] GOSWAMI, R. et al., Phys. Plasmas **8** (2001) 857.
[21] PETRIE, T. W. et al., Nucl. Fusion **37** (1997) 321.
[22] MAINGI, R. et al., Nucl. Fusion **45** (2005) 264.